Ref 23 in Hoster

Surface Science 293 (1993) 67–80
North-Holland

LEIS and AES on sputtered and annealed polycrystalline Pt–Ru bulk alloys

H.A. Gasteiger, P.N. Ross, Jr. and E.J. Cairns
Chemical Engineering Department, University of California at Berkeley, and Lawrence Berkeley Laboratory, Berkeley, CA 94720, USA

Received 18 March 1993; accepted for publication 26 April 1993

Low energy ion scattering spectroscopy (LEIS) and Auger electron spectroscopy (AES) were performed on sputtered and UHV annealed polycrystalline Pt–Ru bulk alloys over the entire compositional range. LEIS spectra were acquired with an estimated sputter damage of less than 0.5% of a monolayer by employing $^4He^+$ ions with an energy of 2 keV and a current density of 20 nA/cm^2. The partial overlap of the scattering peaks of Pt and Ru made it necessary to devise a method to numerically fit the data.

LEIS showed that sputter-cleaning with 0.5 keV Ar^+ ions at 63° incidence does not effect any preferential sputtering. Annealing at 800°C in UHV causes a strong surface enrichment in Pt for equilibrated Pt–Ru alloys. The alloy with a hcp bulk lattice (9.5 at% Pt) exhibited a larger segregation than the fcc alloys (> 35 at% Pt), which we rationalized with the lattice mismatch between the bulk and the surface face structure, resulting in a loosely packed surface. Second-layer compositions of annealed specimens were extracted from AES and LEIS data, utilizing a calibration method based on Auger signals of the continuously sputtered surface. A smooth decay of the enriched outermost layer composition towards the bulk composition was assessed. The platinum surface enrichment of annealed bulk alloys was contrasted with the segregation observed for bimetallic supported clusters of Pt and Ru. Ideal solution thermodynamics, utilizing surface free energy data and molar surface area data from the literature, was able to predict the measured segregation for the UHV annealed bulk alloys.

1. Introduction

Thermodynamic modelling of surface enrichment has become progressively more refined (e.g. refs. [1–5]), as experimental methods have evolved to assess the composition of the outermost surface layers in contrast to the bulk composition of homogeneous alloys. This outermost surface layer composition was soon recognized to be an important factor in determining the activity of alloy catalysts in gas-phase catalysis [6] as well as in electrocatalysis [7]. Auger electron spectroscopy (AES) was one of the first methods applied to the study of surface enrichment phenomena. To quantify Auger signals in terms of atomic percent, calibration spectra are usually taken on elemental standards and in order to account for significant matrix effects in electron backscattering, in-situ fracturing of alloys in ultra-high vacuum (UHV) has been employed [8]. Rather long, and not easily measurable attenuation lengths of Auger electrons (several monolayers), however, still seriously hamper the quantitative analysis of AES data in terms of top-layer compositions [9], rendering angle-resolved AES an important part of signal quantification. The same problem, even more pronounced due to commonly larger attenuation lengths applies to X-ray photoelectron spectroscopy (XPS). Low energy ion scattering spectroscopy (LEIS), discovered in its present form in the late sixties [10], overcomes the difficulties associated with the signal averaging over several atomic layers in AES and XPS. Experiments with monolayers of bromine on silicon [11] as well as many other adsorption studies have established the outstanding sensitivity in LEIS towards the outermost atomic layer. The large cross-section for neutralization of rare gas ions by itinerant electrons in metals is responsible for the excellent surface sensitivity of LEIS [12]. The energy loss due to the elastic scattering of low energy noble gas ions from a clean surface in

UHV can easily be measured with standard electrostatic ion/electron analyzers and is well described by the classical equations for the conservation of energy and momentum.

The present study is aimed at assessing surface and near-surface concentrations of sputtered and annealed platinum–ruthenium alloys by means of AES and LEIS. These alloys are utilized in hydrogenation catalysis and are also the most promising electrocatalysts in the anodic oxidation of methanol [13]. Besides our interest in conjunction with their catalytic activity, Pt–Ru is an alloy system which serves as an interesting test case for thermodynamic models of surface segregation due to the large difference in the heat of sublimation of platinum and ruthenium but very similar atomic radii [14,15].

2. Experimental procedures

Five polycrystalline platinum–ruthenium bulk alloys and specimens of the pure elements were prepared in an arc-melting furnace under argon atmosphere from 99.95% pure materials (Johnson Matthey). They were homogenized by at least 10 melt cycles, followed by homogenization under vacuum at 1600°C for 24 h. All alloys were shown to consist of a single phase via X-ray diffraction and their chemical composition was verified by X-ray fluorescence spectroscopy (±0.5 at%), calibrated with mixtures of platinum and ruthenium black powders (Johnson Matthey). The chemical composition and the lattice constants of the alloys employed in this study are listed in table 1. All alloy specimens were polished with emery paper and mirror-finished with a $\frac{1}{4}$ μm diamond paste (Buehler); before introduction into the UHV they were ultrasonically cleaned in detergent, in pyrodistilled water, and in methanol.

LEIS and AES data were collected in a PHI UHV system with a base pressure of 5×10^{-10} Torr, equipped with an angular-resolving double pass cylindrical mirror analyzer (DPCMA Φ15-255GAR) with an electron source at its center axis. AES data were recorded in a derivative mode with a modulation width of 3 eV selected via a Φ20-805 analyzer control at an electron beam energy of 3 keV; no angular resolved AES measurements were recorded. A digitally controlled Φ32-100 electron multiplier supply in combination with a Φ20-810 analyzer control and an IBM PC were employed for LEIS data acquisition. For the recording of both AES and LEIS data the DPCMA was operated in the constant retard ratio mode. Using the 90° slit in the angular resolving drum of the DPCMA, the signal count rate could be maximized without compromising its resolution, requiring an acquisition time of only one minute per spectrum. A Φ04-303A differentially pumped ion gun was used to raster a 2 keV $^4He^+$-ion beam over an area of approximately 3 mm by 3 mm. Ion beam currents were measured at a positive bias of 95 V and were always less than 20 nA/cm^2 at a residual He pressure of 2×10^{-8} Torr in the UHV chamber. The angle of incidence (angle between the surface and the ion beam) of the $^4He^+$ ions was 45° and the take-off angle was 87° to avoid shadowing effects; the average backscattering angle was 127°. A more detailed description of the employed instrumentation can be found in ref. [16]. Samples were prepared in the UHV via cycles of sputtering with argon ions at an incidence angle of 63° and a beam energy of 0.5 keV, and of annealing at 800°C by means of a resistively heated tungsten filament. For some of the alloy specimens a more elaborate preparation method had to be devised in order to attain UHV annealed surfaces without surface active contaminants (Cu, P and S). These specimens were sputtered with 0.5 keV Ar^+ while being maintained

Table 1
Prepared specimens: composition in at% based on X-ray fluorescence measurements, crystal structure and lattice parameters for fcc (*a*) and hcp (*a* and *c*) lattices measured by X-ray diffraction

	%Pt	Structure	*a* (Å)	*c* (Å)
Pt	100.0	fcc	3.9231	–
PtRu-3	90.3	fcc	3.9166	–
PtRu-5	70.2	fcc	3.8907	–
PtRu-4	48.3	fcc	3.8624	–
PtRu-2	39.4	fcc	3.8486	–
PtRu-6	9.5	hcp	2.7178	4.3140
Ru	0.0	hcp	2.7058	4.2819

at a temperature of 900°C over a period of several days; this cleaning procedure was successful with all samples. Prior to any sample analysis, all specimens introduced into UHV were sputter-cleaned (2 keV Ar^+) followed by annealing at 800°C in UHV for 15 min in order to minimize possible effects of sputter etching. AES spectra from 40 to 540 eV were then recorded before each experiment to verify the absence of surface active contaminants.

3. Results

3.1. LEIS measurements

3.1.1. Calibration and signal deconvolution

Calibration of the ion scattering signals was carried out on pure platinum and pure ruthenium at a total beam current of 100 nA and a He background pressure of 2×10^{-8} Torr, at room temperature. These LEIS signals were carefully maximized by moving the sample across the focal point of the analyzer and the beam current was measured at a sample bias of +95 V in order to suppress the emission of secondary electrons. The scattering peaks of Pt and Ru agreed to within ±0.5% with the value predicted by the classical equation for elastic collisions [17]:

$$\frac{E_1}{E_0} = \frac{1}{[1+(M_2/M_1)]^2} \times \left(\cos\theta + \sqrt{(M_2/M_1)^2 - \sin^2\theta}\right)^2, \quad (1)$$

where M_1 and M_2 are the mass of the incident ion and the target atom, respectively, E_0 is the energy of the incoming ion beam, E_1 is the energy of scattered He ions and θ is the backscattering angle. For our experimental parameters the relative energy loss, E_1/E_0, for ion scattering from platinum and ruthenium is 0.936 and 0.881, respectively. To attain a more accurate agreement with eq. (1), one would need to consider that the average scattering angle of 127° in our experimental arrangement has a deviation of ±6°, based on the use of the 90° slit in the angle resolving aperture of the DPCMA.

In our LEIS experiments we have chosen $^4He^+$ ions because of their extremely low sputtering rates as compared to Ne^+ or Ar^+ ions (approximately a factor of 20 [18,19]), ensuring us of a sputter damage of less than 0.5% of a monolayer during data acquisition. However, with He^+ there is more overlap of the Pt and Ru scattering peaks than with the heavier gases. It was necessary to devise a method to numerically fit the LEIS signals of Pt and Ru to deconvolute the signals. Although several examples of LEIS peak fitting can be found in the literature, e.g. exponentially decaying tails [20,21], we have sought to develop our own fitting equation. This equation outlined in the following has the advantage over, e.g. the fitting with exponentially decaying tails that the initial input parameters are very well defined and easily extracted from a recorded spectrum, whereas it is rather tedious to establish initial guesses for the referenced fitting equations in the literature. Ion scattering signals with $^4He^+$ ions in particular are characterized by a pronounced low energy tail due to inelastic losses to metal electrons [12], therefore we have based our model equation on the assumption that most of the inelastic losses occur by means of surface plasmon excitations. A free electron gas model can predict the energy of volume and surface plasmons [22] and numerical results for Pt and Ru volume plasmons are cited in the literature to be 30.2 and 28.5 eV, respectively [23]. Neither of the two metals is a good example of a free electron material, but inelastic electron beam scattering experiments (1 keV) in our laboratory have yielded values of the volume plasmons for Pt and Ru of 30 and 29 eV, respectively. Since LEIS signals originate from the outermost surface layer, surface plasmons rather than volume plasmons were used in our fitting. In the following, we have approximated the energy of surface plasmons for Pt–Ru alloys, ω_s, with an average value of 20.8 eV, corresponding to $1/\sqrt{2}$ times the value of the measured and averaged bulk plasmons. The expression to fit the measured LEIS spectra of Pt and Ru is then a summation of a main signal at the elastic peak position, E_1, and a decaying series of plasmon modes, all characterized by a

Gaussian profile:

$$Y(E) = c_1\left(\exp\left\{-\frac{1}{2}\left[\frac{E-E_1}{c_2}\right]^2\right\} + c_3\sum_{i=1}^{20}\frac{1}{i+c_4\sqrt{i}} \times \exp\left\{-\frac{1}{2}\left[\frac{E-(E_1-i\omega_s)}{c_2}\right]^2\right\}\right), \quad (2)$$

where $Y(E)$ is the measured ion yield at energy E, c_1 is the overall signal amplitude, c_2 is the width of the Gaussian as determined mainly by the angular resolution of the analyzer (see eq. (1)), c_3 is the tail amplitude and c_4 is an additional tail parameter. The limit on the index i was chosen to be sufficiently large as to extend over the entire energy range, E, where data were acquired. For spectra of pure Pt and pure Ru, a numerical least-squares fitting routine was utilized [24] to evaluate the parameters c_1, c_2, c_3, c_4 and E_1. Results of these fits are shown in fig. 1. The deviation between the numerical fit and the data at the high energy end of the respective spectra most likely derives from multiple scattering events, which have not been considered, but whose effect is negligible for our purposes. LEIS spectra on the alloys were then deconvoluted by fitting eq. (2) to the ion scattering data, with all parameters remaining fixed to their values as assessed above except for c_1 and E_1 for both metals and c_3 for platinum. The numerical values for E_1 did vary by approximately $\pm 0.2\%$, based on the accurate positioning of the sample. Fig. 2 shows a typical fit on an annealed alloy sample with a Pt surface composition of 91.8 ± 3 at%.

Sensitivity factors, $S_{Pt/Ru}$, were derived from the fitted peak height ratios, H_{Pt}/H_{Ru}, extracted from $Y(E)$ (eq. (2)). Values of $S_{Pt/Ru}$ for three independent experiments over the course of three months are shown in table 2, based on [25]:

$$S_{Pt/Ru} = (H_{Pt}/H_{Ru})_{pure}\frac{\sqrt{3/4}\,a_{Ru}^2}{\sqrt{3/16}\,a_{Pt}^2}, \quad (3)$$

where H_{Pt}/H_{Ru} is the intensity ratio measured for the pure elements and a_{Ru} and a_{Pt} are the lattice constants of the elements as listed in table 1 (i.e. molar surface areas are approximated for a (111) surface). Their variance is significantly less than reported in a recent LEIS study on Pt–Cu alloys [25] and results in an average absolute error of ± 2 at% in assigning atomic fractions to LEIS signals, according to:

$$x_{Pt}^{surf} = \frac{S_{Pt/Ru}}{S_{Pt/Ru} + (H_{Pt}/H_{Ru})_{exp}}. \quad (4)$$

Ackermans et al. [26] have reported a different method to attain sensitivity factors in LEIS analysis, based on absolute signal counts rather than intensity ratios. Since, however, we have worked with extremely low ion beam currents (~ 1 nA) in order to avoid sputtering effects, our beam current measurements were accurate only to within $\pm 30\%$, necessitating the use of intensity ratios.

If, as is commonly assumed, matrix effects in LEIS signals are negligible, the ratio of the differential cross-sections of Pt and Ru should correspond to the ratio found in the above calibra-

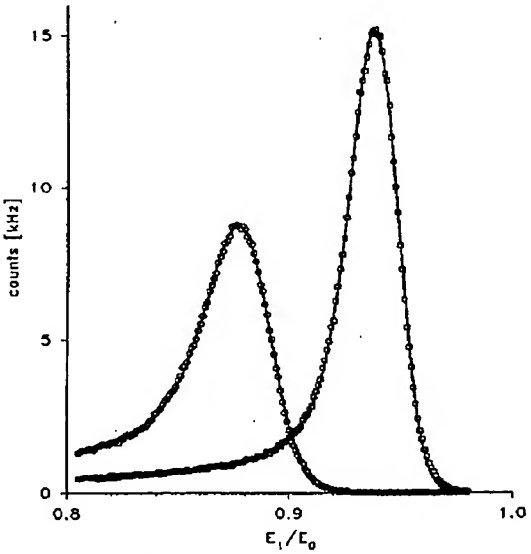

Fig. 1. $^4He^+$ LEIS (2 keV) on pure Pt (□) and pure Ru (○) at a beam current of 15 nA/cm^2. The beam was rastered over an area of 3 mm by 3 mm. The solid lines are least-squares fits according to eq. (2) in the text.

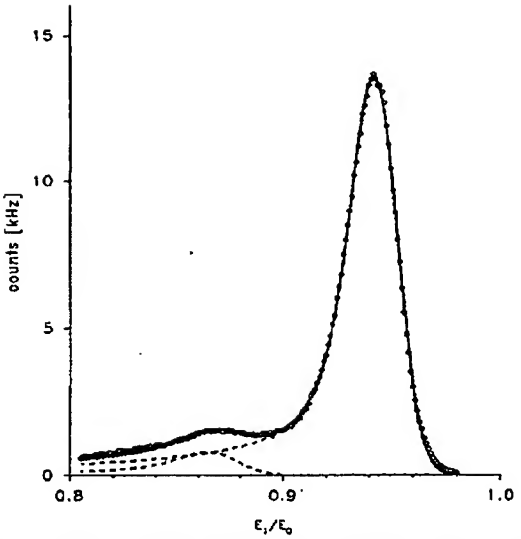

Fig. 2. $^4He^+$ LEIS (2 keV) on an annealed Pt–Ru alloy (PtRu-5) at a beam current of 18 nA/cm^2. The beam was rastered over an area of 3 mm by 3 mm: (○) raw data; (———) least-squares fit.

tion, if the analyzer transmission function is accounted for. Differential cross-sections for LEIS can be calculated classically by assuming a potential energy function for the colliding atoms, e.g. a screened Coulomb potential [27,28]. For the parameters in our experiment, we have calculated the ratio of differential cross-sections of Pt to Ru to be 1.36. By approximating the DPCMA transmission function for the constant retard ratio mode by a $\sqrt{E_1}$ functionality, the LEIS sensitivity factor for Pt and Ru, $S_{Pt/Ru}$, is calculated to be 1.41, which is very close to the measured values (see table 2).

Table 2
Sensitivity factors, $S_{Pt/Ru}$, for three independent experiments on Pt and Ru standards (see eq. (3)): 2 keV $^4He^+$ ion beam, 100.0 nA/cm^2, room temperature, $\theta = 127°$

$S_{Pt/Ru}$			Average $S_{Pt/Ru}$
1.52	1.64	1.38	1.51 ± 0.13

Table 3
Surface compositions (at%) of sputtered alloys (0.5 keV Ar^+) as determined by LEIS for two independent sets of experiments, and AES peak-to-peak ratios based on Auger transition energies as indicated by the subscripts

	x_{Pt}^{surf}	$(Pt_{64}/Ru_{273})_{AES}$	$(Ru_{273}/O_{503})_{AES}$
Data set 1			
PtRu-3	94.4	12.2	–
PtRu-5	67.5	2.88	–
PtRu-4	54.4	1.26	–
PtRu-2	44.5	0.78	60
PtRu-6	14.4	0.105	50
Data set 2			
PtRu-3	91.7	12.2	–
PtRu-5	66.1	3.11	–
PtRu-4	53.1	1.24	–
PtRu-2	44.9	0.81	55
PtRu-6	13.3	0.095	65

3.1.2. Surface composition of sputtered alloys (0.5 keV Ar^+)

It is well established that sputtering of bimetallic surfaces in UHV may produce surface enrichment in one of the components if the atomic sputtering yields (number of sputtered surface atoms per sputtering ion) are significantly different from each other (e.g., in the Cu–Ni system). In conjunction with our research on the electrocatalytic activity of sputtered Pt–Ru alloys towards the oxidation of methanol [29], we investigated here the relationship between bulk and surface concentration for sputter-cleaned Pt–Ru alloys. Alloy specimens were bombarded with 0.5 keV Ar^+ ions at an angle of incidence of 63° and at a current density of approximately 10 μA/cm^2 for 15 min. Sputtering over longer periods of time did not affect the results of LEIS and AES experiments. The cleanliness of the prepared surfaces was verified via AES for each measurement in two independent sets, which are listed in table 3 and summarized in fig. 3 and which exhibit excellent reproducibility. The amount of oxygen present on the two alloys with a high Ru bulk concentration is estimated to be at most 10% of the Ru atomic fraction, as inferred from AES peak-to-peak ratios of Ru and oxygen [30]. No reduction in ion scattering yields was observed in these cases. It is clear from fig. 3 that, under the above

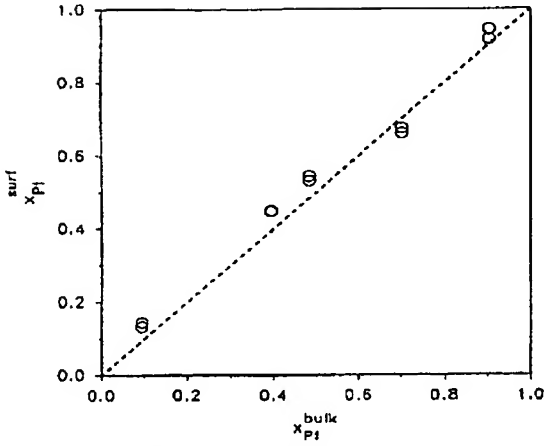

Fig. 3. Pt surface and bulk compositions of sputtered Pt–Ru alloys as determined by LEIS. Sputtering conditions: 0.5 keV Ar^+ at 63° angle of incidence.

conditions, surface and bulk composition of sputtered Pt–Ru alloys are essentially identical within the accuracy of the measurement. Published data on the sputter yields of pure platinum and pure ruthenium at normal incidence of 0.5 keV Ar^+ ions [19] would predict a slight enrichment of Ru based on a sputter yield ratio of Pt to Ru of 1.3. Sputter yields at approximately 60° incidence, however, are up to 100% larger than those at normal incidence [31] and sputter yield ratios are expected to change significantly with the angle of incidence.

3.1.3. *Surface compositions of annealed alloys (800°C in UHV)*

After sputter-cleaning Pt–Ru alloys were annealed in UHV at 800°C for periods of 15 or 30 min and data for two independent sets of experiments are listed in table 4. In studying the surface segregation of these alloys it was imperative to ascertain whether equilibrium was attained under the conditions of the experiment. Starting out with the equilibrium sputtered surface of one alloy sample (PtRu-6, which has the highest melting point) at 25°C, we raised the temperature to 800°C and recorded its surface composition at various times. Although the sensitivity factor,

Table 4
Surface compositions (at%) of annealed alloys (800°C) in UHV) as determined by LEIS for two independent sets of experiments, and AES peak-to-peak ratios based on Auger transition energies as indicated by the subscripts

	x_{Pt}^{surf}	$(Pt_{64}/Ru_{273})_{AES}$	$(Ru_{273}/O_{503})_{AES}$
Data set 1			
PtRu-3	> 96	26.7	–
PtRu-5	92.1	6.18	–
PtRu-4	88.4	3.66	–
PtRu-2	84.8	2.46	–
PtRu-6	90.6	0.98	–
Data set 2			
PtRu-3	> 96	30.9	–
PtRu-5	91.8	6.45	–
PtRu-4	88.3	3.36	–
PtRu-2	84.6	2.54	–
PtRu-6	90.3	0.96	–

$S_{Pt/Ru}$, is based on room temperature measurements, it is not expected to significantly change with temperature (this assumption based on theoretical considerations is confirmed in a study on Pt–Rh alloys by Beck et al. [32]). The experimental data in fig. 4 verify the establishment of equilibrium within 10 min for the highest-melting

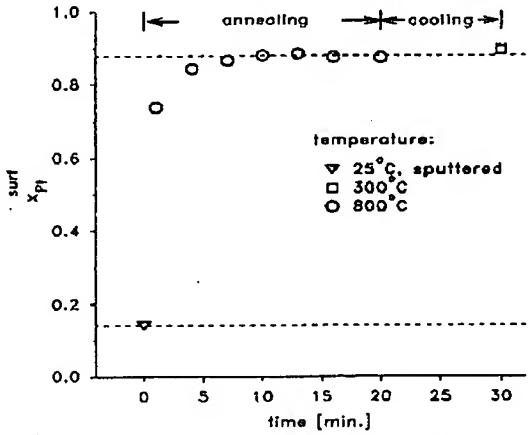

Fig. 4. Surface composition of the PtRu-6 alloy sample as a function of annealing time at 800°C, and after sample cooling. Prior to this experiment the surface was sputtered with 0.5 keV Ar^+ ions. The average surface compositon of the annealed and the sputtered alloy is indicated by dashed lines.

alloy in our study. All other segregation measurements reported here were recorded after sample cooling to room temperature, at initial cooling rates of 200°C/min, reaching 500°C in less than two minutes. For temperatures below 500°C, the equilibration is very slow (> 1 h) and so the error introduced by cooling the samples prior to analysis was expected to be negligible, as confirmed by fig. 4. The slight increase in surface enrichment for the cooled sample is consistent with predictions of theoretical equilibrium models presented in a later section (4.2).

The equilibrium surface compositions of four Pt–Ru alloys are plotted in fig. 5 together with theoretical predictions which will be discussed later. The surface enrichment in platinum is quite significant and does behave in a systematic fashion for the fcc structure alloys. The alloy with the largest platinum content (PtRu-3) yielded a surface composition above 96 at% and since we could not assign a more definite numerical value it is indicated by a plain error bar in fig. 5. Apparently different behavior is exhibited by the alloy with the hexagonal crystal structure (hcp) at

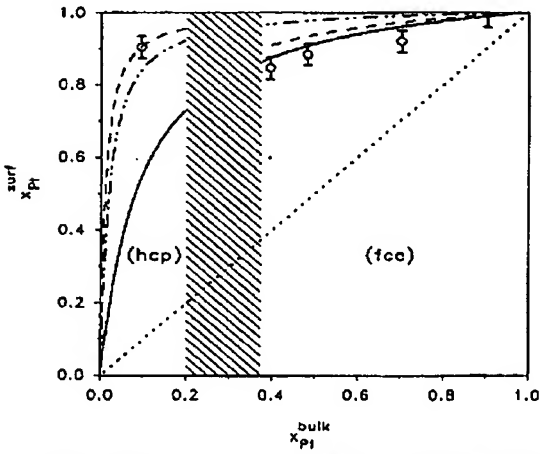

Fig. 5. Experimental data of Pt–Ru alloys annealed at 800°C in UHV (○). Thermodynamic monolayer model by Strohl and King [55] for different low-index planes: (———) fcc (111) and hcp (0001); (– · · – · · –) fcc (110) and hcp (11$\bar{2}$0); (- - - - - -) fcc (100) and hcp (10$\bar{1}$0); (· · · · · ·) diagonal; (\\\\\\) indicates the two-phase region of the bulk alloy.

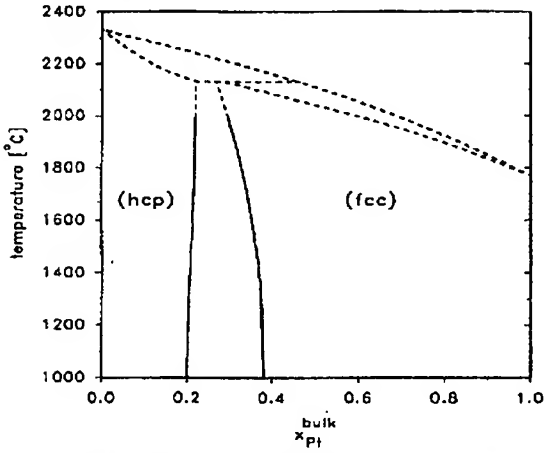

Fig. 6. Phase diagram of the platinum–ruthenium system (reproduced from J.M. Hutchinson [33]).

a bulk composition of 9.5 at% platinum, where the platinum surface enrichment seems too large in comparison with the other alloy samples. According to the bulk phase diagram of the platinum–ruthenium system (reproduced from Hutchinson [33]), fig. 6, the hcp alloy (PtRu-6) reaches a surface composition which, in the bulk would correspond to a fcc lattice. The additional driving force for segregation established by this crystal structure mismatch may be responsible for the very strong enrichment observed in this alloy. Embedded atom calculations for the Co–Ni system (Ni has an fcc structure and Co crystallizes in an fcc lattice) have predicted a very strong surface enrichment in Ni, although heats of sublimation and atomic radii of these two elements are very nearly identical [34]. This will be discussed in more detail in section 4.2.

3.2. AES measurements

In contrast to the outermost-layer information provided by LEIS, AES signals incorporate information from several atomic layers with a depth-distribution along the surface normal (z-axis) characterized by the mean free path of Auger electrons, $\lambda(E)$, at energy E. Typical AES spec-

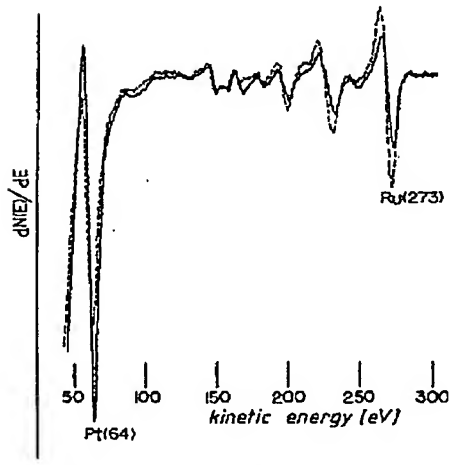

Fig. 7. AES spectra of PtRu-5 recorded in the derivative mode: (———) annealed at 800°C in UHV; (- - - - -) sputtered with 0.5 keV Ar^+ ions.

tra of an annealed and a sputtered Pt–Ru alloy are compared in fig. 7. The overall intensity is a well-defined function of the depth-distribution of the electron emitting element, $N_A(z)$, the impinging electron beam current, I_0, with energy E_p, the roughness factor of the specimen, ρ, the Auger cross-section, $\sigma(E_p)$, the matrix-dependent backscattering factor, R_M, the transmission function of the analyzer, $T(E)$, and the detector efficiency, $D(E)$. The attenuation length of Auger electrons is defined by the product of their mean free path and the cosine of the angle of emission with respect to the surface normal, α. The mathematical description (e.g. see Rivière [17]) of an Auger signal from element A, I_A, is then:

$$I_A = I_0 \rho \sigma_{A(E_p)} R_M T_{(E)} D_{(E)} \int_\phi \int_\beta \int_0^\infty N_{A(z)} \times \exp\left(\frac{-z}{\lambda_A \cos\alpha}\right) dz \sin\beta\, \beta\, d\beta\, d\phi, \quad (5)$$

where β is the acceptance angle of the analyzer (42.3° ± 6° for the DPCMA) and ϕ is the rotation angle about the analyzer axis. For our experimental set-up, with the sample being mounted at 45° with respect to the analyzer axis, cos α is defined as:

$$\cos\alpha = \frac{1}{\sqrt{2}}(\cos\phi \sin\beta + \cos\beta). \quad (6)$$

Since neither Auger cross-sections nor backscattering factors can be calculated from first principles with sufficient accuracy, signal calibration is of essential importance in AES. The most accessible calibration method is based on elemental standards while recording Auger peaks at different energies to attain depth-distribution information [35]. Here it is crucial to reproduce precisely the sample alignment, electron beam current and surface roughness for each sample. A more cumbersome, yet very powerful procedure is the in-situ fracturing of an alloy specimen in order to create a homogeneous distribution of its components along the z-axis [8]. In our experiments we have attempted to employ a very similar calibration method based on the LEIS results on sputtered alloy surfaces (see section 3.1.2), which were shown to have identical bulk and surface concentrations within the accuracy of the measurement. Knowing that N_{Pt} and N_{Ru} are independent of z for sputtered alloys, eq. (5) simplifies to:

$$\frac{I_{Pt}}{I_{Ru}} = \frac{\sigma_{Pt(E_p)} R_{M(E_{Pt})} T_{(E_{Pt})} D_{(E_{Pt})} \lambda_{(E_{Pt})}}{\sigma_{Ru(E_p)} R_{M(E_{Ru})} T_{(E_{Ru})} D_{(E_{Ru})} \lambda_{(E_{Ru})}} \frac{x_{Pt}}{x_{Ru}}. \quad (7)$$

This may be rewritten as:

$$\frac{I_{Pt}}{I_{Ru}} = K \frac{x_{Pt}}{x_{Ru}}. \quad (8)$$

Since the bulk atomic fractions are known, the Auger intensity ratios in table 3 will facilitate the evaluation of the calibration factor K, varying by approximately ±5% for each sample. The only matrix dependent variables in K are the backscattering factors, R_M, and the electron mean free paths. The former characterizes the enhancement of the impinging electron beam via elastic backscattering of high energy electrons ($\sim E_p$) and is to a very good approximation a function of the bulk matrix composition only [36].

The inelastic mean free path of electrons is most commonly evaluated using the "universal curve" compiled by Seah and Dench [37]. Based mainly on overlayer experiments, a functional relationship between λ and electron energy was established for the elements, ignoring matrix effects and resulting in a root mean square scatter factor of 1.59. Recent inelastic mean free path (IMFP) calculations [23] for electrons by means of optical data provide a more accurate assessment of the mean free path of electrons as it is applicable to AES experiments. From these calculations we have derived the IMFP at 64 eV kinetic energy (corrected for the work function of the analyzer) in platinum and ruthenium to be 4.34 and 4.33 Å, respectively; the values at a kinetic energy of 273 eV are 5.80 and 6.32 Å, respectively. The matrix effect in the IMFP is quite small considering the precision claimed by Tanuma et al. [23] and we have applied arithmetic averages at each electron energy for our calculations. The values at 273 eV are markedly lower than the prediction given by the "universal curve", significantly affecting AES model calculations. It should be noted that because of the contribution of elastic electron scattering the IMFP should be considered as the upper limit for the electron mean free path [38].

UHV annealed Pt–Ru alloys exhibit a first layer composition strongly enriched in platinum, as evidenced by our ion scattering analysis. Therefore, the composition of near surface layers is a function of their position along the z-axis, expressed as $N_A(z)$ in eq. (5), which may be integrated layer by layer:

$$\frac{I_{Pt}}{I_{Ru}} = K\left[x_{Pt}^{(1)}\int_\phi\int_\beta \cos\alpha\,\sin\beta\,d\beta\,d\phi + \sum_{i=1}^{\infty}\left(x_{Pt}^{(i+1)}-x_{Pt}^{(i)}\right)\times\int_\phi\int_\beta \exp\left(\frac{-id}{\lambda_{Pt}\cos\alpha}\right)\times\cos\alpha\,\sin\beta\,d\beta\,d\phi\right]\times\left[x_{Ru}^{(1)}\int_\phi\int_\beta \cos\alpha\,\sin\beta\,d\beta\,d\phi + \sum_{i=1}^{\infty}\left(x_{Ru}^{(i+1)}-x_{Ru}^{(i)}\right)\times\int_\phi\int_\beta \exp\left(\frac{-id}{\lambda_{Ru}\cos\alpha}\right)\times\cos\alpha\,\sin\beta\,d\beta\,d\phi\right]^{-1}. \quad (9)$$

Here, the mole fractions of platinum and ruthenium are expressed for each layer, i ($i = 1$ is the outermost surface layer, $i = \infty$ refers to the bulk compositon), and the average distance between crystal planes of a polycrystalline specimen, d, derived from molar volumes is 2.34 Å. Assuming the above values for the mean free paths of Auger electrons emitted from platinum (64 eV) and from ruthenium (273 eV, also see fig. 7), the angular integrals in eq. (9) in conjunction with eq. (6) are easily evaluated by numerical integration. Thus, we find that 79% of the platinum Auger signal and 67% of the ruthenium Auger signal stem from the first and the second layer. Given the large signal contribution from the two outermost atomic layers, we have extracted second layer compositions from our Auger data by fixing the first layer composition to the values found by LEIS (see table 4) and by assigning the sample's bulk composition from the third layer on. The latter assumption is based on the fact that nearly ideal solutions will approach bulk composition within a few atomic layers; that the Pt–Ru system behaves very closely to an ideal solution will be shown in section 4.2. Thus, eq. (9) simplifies to:

$$\frac{I_{Pt}}{I_{Ru}} = K\left[0.4604x_{Pt}^{(1)} + 0.2034\left(x_{Pt}^{(2)}-x_{Pt}^{(1)}\right) + 0.1008x_{Pt}^{(\infty)}\right]\times\left[0.4604x_{Ru}^{(1)} + 0.2513\left(x_{Ru}^{(2)}-x_{Ru}^{(1)}\right) + 0.1492x_{Ru}^{(\infty)}\right]^{-1}, \quad (10)$$

where K, as discussed above is a constant evaluated for each alloy sample, depending on its bulk composition only. Second layer compositions of annealed alloys derived from eq. (10) are plotted together with the LEIS data in fig. 8. The error bars are based on the estimated accuracy of K ($\pm 5\%$), the precision of Auger peak-to-peak intensities ($\pm 5\%$ experimentally observed scatter),

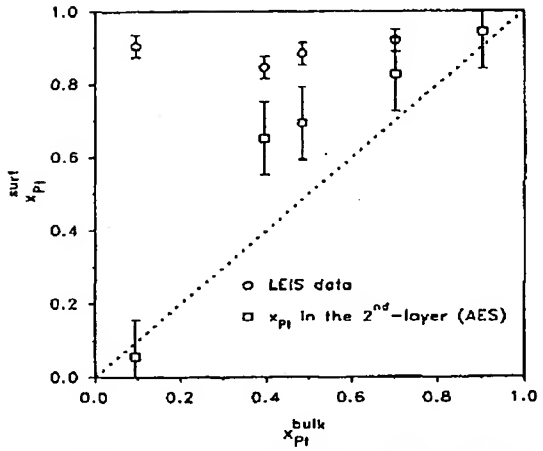

Fig. 8. First and second layer platinum surface composition of annealed Pt–Ru alloys: (○) LEIS data; (□) second layer composition derived from AES; (·····) diagonal.

the variation of the distance between different at planes (±15% for low index planes), and the uncertainty in the mean free paths of Auger electrons (±13%, ref. [23]). Fig. 8 indicates the second layer composition to still be significantly different from the bulk composition and our previous assumption, viz. that the third layer would already be very close to the bulk compositon may not be correct. Nevertheless, the error introduced by this factor is expected to be small because the main contribution to the Auger signals does originate from the first two atomic layers as outlined above. In principle, measuring Auger transitions at different energies, eq. (9) can be utilized to solve for more than two atomic layers (e.g. see ref. [35]). Unfortunately, all other Pt and Ru Auger transitions below 1000 eV overlap and we did not use the high energy transition of platinum at 1967 eV [39] because of its long IMFP of approximately 20 Å.

4. Discussion

4.1. Comparison with literature data

The literature on surface segregation phenomena of Pt–Ru bulk alloys is very scarce and even for supported bimetallic clusters not much has been published. A photoemission study of Pt–Ru bulk alloys with up to 55 at% ruthenium was reported by Hilaire et al. [40]. Its results, which show very little platinum surface enrichment, are in stark contrast to our data. A major error in attempting to quantify their measurements in terms of atomic percent, is their approach of plainly using sensitivity factors in their XPS (X-ray photoelectron spectroscopy) signal analysis. The inelastic mean free paths of Pt and Ru photoelectrons (Al anode) are 17 Å [23], and signals will be averaged over approximately 10 atomic layers, which clearly invalidates their assumption of attaining first layer information without more refined signal processing or angle-resolved measurements. Ticanelli et al. [41] report $^{20}Ne^{+}$ ion scattering on a 50 at% Pt–Ru bulk alloy subjected to voltammetric cycling, but no attempt was made to quantify LEIS signals. A recent time-of-flight (TOF) atom-probe analysis by Tsong et al. [42] investigated the (001) face of a Pt–Ru alloy (17.7 at% Ru), which had been annealed in UHV at 700°C for 15 min. The reported first layer platinum composition of approximately 93 at% is in very good agreement with our findings (see fig. 5). In their study, the bulk composition is reached in the third layer, but the reported second layer composition (~ 76%) would imply an oscillatory behavior which is at variance with our AES data analysis (see fig. 8). However, it is very likely that 5 min at 700°C were not sufficient to warrant the establishment of equilibrium over several atomic layers, so that their measurement would reflect a transient state rather than equilibrium. In support of this, we refer to fig. 4 which shows that equilibration even at 800°C requires approximately 5 min. Diffusivities of solids change very drastically with temperature, e.g. the diffusivity of platinum in platinum at 700°C is more than a factor of 20 smaller than the value at 800°C [15], decreasing its diffusion length by a factor of 4.5, and so we believe that complete equilibration has not been achieved in this study by Tsong and coworkers. In an older study by the same author [43] "equilibration" of a Pt–Ru alloy had been carried out at 800°C for 15 s and no segregation was observed.

Bimetallic supported catalysts are the very basis of industrial catalysis. Very common support materials are, e.g., carbon, alumina and silica. Surface enrichment of Pt–Ru clusters on either alumina or silica was investigated by Miura et al. [44]. Support materials were coimpregnated with Pt and Ru salts, reduced in hydrogen and annealed in vacuum at 450°C. All samples, over the entire compositional range exhibited surface enrichment of platinum as measured by O_2–CO surface titration (~ 80% Pt for a 50% bulk composition on both alumina and silica). For clusters diluted in one of the components, the authors report different behavior depending on the nature of the support, which they rationalize by metal–support interaction. It is stated that dispersions (ratio of the number of surface atoms to the number of bulk atoms) of catalysts supported on silica are larger than of those supported on alumina, with the dispersion for bimetallics ranging from 17% to 60%. At high dispersion, a large fraction of the atoms in a particle (~ 10 to 25 Å) are located on the surface and the internal composition, i.e. "bulk composition", changes significantly if surface segregation occurs, necessarily leading to cherry-model like structures. Thus, one would expect large differences in the surface compositions of clusters on different substrates when there is a large variation in the dispersion. The dispersion of metals on supports is a strong function of the reducing conditions during cluster preparation, the nature of the metal precursors, and the substrate [45,46], and in our view it is the effect of the substrate on dispersion that is the cause of the difference in surface composition for Pt–Ru on silica versus alumina. In order to be able to compare platinum enrichment found in the supported clusters with that found here, the comparison should only be made at a sufficiently low dispersion and at sufficiently small surface enrichment such that segregation is not affecting a large fractional change in the cluster's bulk composition. Bulk and surface compositions of Pt–Ru clusters were reported by Miura et al. [44] and for samples for which the above conditions were satisfied the agreement with our data is excellent.

4.2. Thermodynamic equilibrium model

The first thermodynamic models to assess the compositonal difference between a surface monolayer and the bulk of a binary ideal solution were developed by Butler [47] and Schuchowitzky [48]. Guggenheim [49] extended their formalism to incorporate regular solution behavior, but Defay et al. [50] proved this approach to be at variance with the Gibbs adsorption isotherm and showed that more than one surface layer was necessary to thermodynamically account for non-ideal solutions. The "quasichemical" approach [51] to model surface segregation is based on bond-breaking considerations and Williams et al. [1] have derived a formalism accounting for four surface layers. For non-ordering binary alloys they have shown the monolayer model to be sufficient, if ideal solution behavior is assumed. If, however, enthalpy of mixing data are utilized to approximate regular solution behavior, the composition varies through more than one layer, in agreement with ref. [50]. In either case, the extent of surface enrichment is strongly dependent on the exposed crystal face, viz. the number of broken bonds at the surface. For ordering alloys, the entropy of mixing must be evaluated differently as was outlined by van Santen et al. [52]. Effects of lattice strain due to different atomic radii of the components in a binary alloy were discussed by Wynblatt and Ku [53]. A monolayer model for binary transition metal alloys, incorporating surface free energies, enthalpies of mixing and at size differences was proposed by Miedema [54]. More recently Strohl and King [55] have developed a thermodynamic multilayer, multi-component model applicable to non-random, non-regular solutions, provided the alloy's mixing properties are known. Besides these, the most important input parameters for both the thermodynamic and the bond-breaking models are surface free energies whose measurement is very difficult for solids and prone to large errors [2]. Therefore, Overbury et al. [3] devised a method for estimating these parameters from enthalpy of sublimation data (e.g. ref. [14]). Based on more refined thermodynamic considerations, Tyson and Miller [56] have

predicted temperature-dependent surface free energies for a large number of solid elements for which the surface tension of the liquid at the melting point was available. Their evaluations are based on estimating surface entropies and they were able to show very good agreement of extrapolated surface free energies at 0 K with bond strengths assessed from enthalpies of sublimation at 0 K; a slightly different approach was taken by Mezey and Giber [57]. The variations in surface segregation calculations depending on both the selection of the model and on the parameters were investigated by Kelley [58]. A very recent development in the calculation of the thermodynamics of surface segregation is the embedded atom method. This mathematically quite elaborate treatment makes use of a Monte Carlo simulation method and is thus able to yield configurational distributions on an alloy surface rather than merely net surface compositions (e.g. ref. [34]). Excellent reviews of surface segregation modelling are provided in refs. [4,5].

In calculating the equilibrium surface composition of annealed Pt–Ru alloys we have employed the thermodynamic model proposed by Strohl and King [55]. Surface free energies at 800°C were estimated according to ref. [56]; their numerical values for platinum and ruthenium are 2.38 and 2.93 J/m^2, respectively. Molar areas of both elements were evaluated from molar volumes and structure factors according to Tyson [59], and are summarized in table 5 for different low-index faces of fcc and hcp lattices. Surface areas for different crystal faces derived from lattice parameters of pure platinum and pure ruthenium (see table 1) are identical to those based on molar volumes and structure factors. Enthalpy of mixing data has never been measured for the Pt–Ru system. A semi-quantitative estimate of the enthalpy of mixing for PtRu was given by Miedema [60] to be −2 kJ/mol. His predictions for all binary transition metal alloys lie within a range of approximately ±100 kJ/mol and he claims that values close to zero would imply the absence of intermetallic phases and good miscibility, which is congruent with the Pt–Ru phase diagram (see fig. 6). Miedema showed that large predicted values of the enthalpy of mixing agreed well with measurements, whereas values close to zero could not be assessed very precisely. For this reason and since the estimated enthalpy of mixing for our system is very small compared to the difference in molar surface free energies of platinum and ruthenium, we have decided to simulate surface segregation with an ideal solution model. The extent to which Vegard's law is obeyed by the fcc structure Pt–Ru alloys (see table 1) is indeed indicative of a closely ideal solution.

Table 5
Molar surface areas of platinum and ruthenium for different low-index surfaces of hcp and fcc structures (in m^2/mol) (numerical values are based on structure factors [59] and molar volumes)

	Platinum	Ruthenium
fcc (111)	4.01×10^4	3.75×10^4
fcc (100)	4.64×10^4	4.33×10^4
fcc (110)	6.55×10^4	6.12×10^4
hcp (0001)	4.01×10^4	3.75×10^4
hcp (11$\bar{2}$0)	6.55×10^4	6.12×10^4
hcp (10$\bar{1}$0)	7.58×10^4	7.08×10^4

With these assumptions, the equilibrium condition according to Strohl et al. does predict only the outermost layer composition, $x_{Ru}^{(1)}$ and $x_{Pt}^{(1)}$, to be different from the bulk composition, $x_{Pt}^{(\infty)}$ and $x_{Ru}^{(\infty)}$.

$$\gamma^{(1)} = \gamma_{Pt}^{(1)}\frac{A_{Pt}^{(1)}}{\bar{A}_{Pt}^{(1)}} + \frac{RT}{\bar{A}_{Pt}^{(1)}}\ln\left(\frac{x_{Pt}^{(1)}}{x_{Pt}^{(\infty)}}\right)$$

$$= \gamma_{Ru}^{(1)}\frac{A_{Ru}^{(1)}}{\bar{A}_{Ru}^{(1)}} + \frac{RT}{\bar{A}_{Ru}^{(1)}}\ln\left(\frac{x_{Ru}^{(1)}}{x_{Ru}^{(\infty)}}\right), \qquad (11)$$

where $A_i^{(1)}$ and $\bar{A}_i^{(1)}$ represent molar and partial molar areas of Pt and Ru, and $\gamma^{(1)}$ and $\gamma_i^{(1)}$ are the outermost layer surface free energy and the pure component's surface free energy, respectively. Partial molar areas may be evaluated from the change of lattice parameters with alloy composition, thereby accounting for lattice strain effects. Using the data in table 1 we found the maximum deviation of partial molar areas from molar areas to be approximately 5%. Considering the vastly varying molar areas for different sur-

face faces (see table 5), we decided to neglect differences between partial molar and molar areas in eq. (11).

Surface composition calculations for different Pt–Ru alloy surface faces of the hcp and fcc structure at 800°C are plotted in fig. 5 together with experimental LEIS data. The two-phase region in the bulk phase diagram is indicated by the hatched area (also see fig. 6). Ideally, minimization of the overall surface free energy is achieved by minimizing the number of broken bonds at the surface, implying that equilibrated surfaces should exhibit low-index faces (this was found, e.g. for polycrystalline Ag–Au alloys [35]). The lowest number of broken bonds in an fcc lattice occurs for a (111) surface with only 25% of the nearest neighbor bonds being ruptured. Thus, the best fit to the experimental LEIS data in the fcc alloys is achieved by assuming a surface area corresponding to a (111) crystal face. The hcp alloy with a very high bulk concentration of ruthenium (PtRu-6) exhibits a surface platinum concentration corresponding to an fcc bulk structure. This lattice mismatch, we believe, is effecting a very loosely packed surface, approximated by a hcp $(10\bar{1}0)$ surface (see fig. 5). The increase in molar area for this structure is characterized by a large fraction of broken surface bonds, viz. 50%. This effectively increases the difference between the molar surface free energies of platinum and ruthenium, enhancing surface segregation.

The second-layer information we have extracted by means of AES does point towards a deviation of the system from ideality, since the composition of the second surface layer is significantly different from the bulk composition, as shown in fig. 8. A small positive enthalpy of mixing would predict this behavior. We have already mentioned the lack of thermodynamic mixing data for the platinum-ruthenium system and so we do not attempt to extend the model in eq. (11) to regular solution theory at the present time. To extend the equilibrium model to highly dispersed bimetallic clusters (see section 4.1) a mass balance in addition to the equilibrium equation would be necessary.

5. Conclusions

$^4He^+$ LEIS indicates that sputter-cleaning of polycrystalline Pt–Ru bulk alloys with 0.5 keV Ar^+ ions at ca. 60° incidence does not effect any preferential sputtering.

Annealing of these alloys in UHV at 800°C produces a strong surface segregation of platinum. Using first-layer compositions from LEIS data and by employing a calibration method for AES signals based on measurements on the continuously sputtered alloy, we were able to extract second-layer compositions. These compositions indicated that platinum surface enrichment of annealed Pt–Ru alloys follows a smooth decay from the outermost layer to the bulk and does not exhibit any oscillatory behavior.

Segregation for the annealed Pt–Ru alloys is described well by ideal solution thermodynamics with surface free energies and molar areas as input parameters. The best fit to the surface versus bulk composition curve for the alloys having the fcc structure (> 38 at% Pt) was produced by using the molar area for a (111) face. The very strong surface segregation observed for the hcp bulk alloy (9.5 at% Pt) is predicted by assuming a relatively open surface face $(10\bar{1}0)$, which appears to be a result of the apparent mismatch of the bulk hcp structure and the fcc structure the surface planes would have if they were bulk planes.

Acknowledgments

At this point we would like to thank Lee Johnson and Bob Wright for their invaluable assistance in building and maintaining the experimental apparatus. Further thanks go to Nenad Marković for his stimulating discussions.

This work was supported by the Assistant Secretary for Conservation and Renewable Energy, Office of Transportation Technologies, Electric and Hybrid Propulsion Division of the US Department of Energy under Contract No. DE-AC03-76SF00098.

References

[1] F.L. Williams and D. Nason, Surf. Sci. 45 (1974) 377.
[2] L.E. Murr, Interfacial Phenomena in Metals and Alloys (Addison-Wesley, Reading, MA, 1975).
[3] F.H. Overbury, P.A. Bertrand and G.A. Somorjai, Chem. Rev. 75 (1975) 547.
[4] W.M.H. Sachtler and R.A. van Santen, Appl. Surf. Sci. 3 (1979) 121.
[5] T.S. King, in: Surface Segregation Phenomena, Eds. P.A. Dowben and A. Miller (CRC Press, Boca Raton, FL, 1990) p. 27.
[6] J.H. Sinfelt, Bimetallic Catalysts (Wiley, New York, 1983).
[7] B.D. McNicol and R.T. Short, J. Electroanal. Chem. 81 (1977) 249.
[8] R. Bouwman, L.H. Toneman, M.A.M. Boersma and R.A. van Santen, Surf. Sci. 59 (1976) 72.
[9] C.J. Powell and M.P. Seah, J. Vac. Sci. Technol. A 8 (1990) 735.
[10] D.P. Smith, J. Appl. Phys. 38 (1967) 340.
[11] H.H. Brongersma and P.M. Mul, Surf. Sci. 35 (1973) 393.
[12] E.P. Suurmeijer and A.L. Boers, Surf. Sci. 43 (1973) 309.
[13] J.-M. Leger and C. Lamy, Ber. Bunsenges. Phys. Chem. 94 (1990) 1021.
[14] R. Hultgren, P.D. Desai, D.T. Hawkins, M. Gleiser, K.K. Kelley and D.D. Wagman, Selected Values of the Thermodynamic Properties of the Elements (American Society for Metals, OH, 1973).
[15] C.J. Smithells and E.A. Brandes, Metals Reference Book (Butterworths, London, 1976).
[16] Physical Electronics Product Bulletin P8301 (Perkin-Elmer, Eden Prairie, MN, 1983).
[17] J.C. Rivière, Surface Analytical Techniques (Oxford University Press, Oxford, UK, 1990).
[18] D. Rosenberg and G.K. Wehner, J. Appl. Phys. 33 (1962) 1842.
[19] N. Laergreid and G.K. Wehner, J. Appl. Phys. 32 (1961) 365.
[20] J.-M. Beuken and P. Bertrand, Surf. Sci. 162 (1985) 329.
[21] V.Y. Young, G.B. Hoflund and A.C. Miller, Surf. Sci. 235 (1990) 60.
[22] C. Kittel, Introduction to Solid State Physics (Wiley, New York, 1986).
[23] S. Tanuma, C.J. Powell and D.R. Penn, Surf. Interface Anal. 17 (1991) 911.
[24] Non-Linear Curve-Fitting Software PeakFit 3.1., Jandel Scientific (1991).
[25] W.L. Baun, in: Quantitative Surface Analysis of Materials, ASTM STP 643, Ed. N.S. McIntyre (American Society for Testing and Materials, OH, 1978) p. 150.
[26] P.A.J. Ackermans, G.C.R. Krutzen and H.H. Brongersma, Nucl. Instrum. Methods B 45 (1990) 384.
[27] E. Everhart, G. Stone and R.J. Carbone, Phys. Rev. 99 (1955) 1287.
[28] F.W. Bingham, Sandia National Laboratory Report SC-RR-66-506 (National Bureau of Standards, Springfield, VA, 1966).
[29] H.A. Gasteiger, N. Marković, P.N. Ross, Jr. and E.J. Cairns, J. Phys. Chem., submitted.
[30] F.M. Hoffmann, M.D. Weisel and C.H.F. Peden, Surf. Sci. 253 (1991) 59.
[31] H. Oechsner, Appl. Phys. 8 (1975) 185.
[32] D.B. Beck, C.L. DiMaggio and G.B. Fisher, General Motors Research Publication GMR-7798 (1992).
[33] J.M. Hutchinson, Jr., Platinum Met. Rev. 16 (1972) 88.
[34] S.M. Foiles, in: Surface Segregation Phenomena, Eds. P.A. Dowben and A. Miller (CRC Press, Boca Raton, FL, 1990) p. 103.
[35] T.S. King and R.G. Donnelly, Surf. Sci. 151 (1985) 374.
[36] M.P. Seah, in: Practical Surface Analysis, Eds. D. Briggs and M.P. Seah (Wiley, New York, 1983) p. 181.
[37] M.P. Seah and W.A. Dench, Surf. Interface Anal. 1 (1979) 2.
[38] A. Jablonski and S. Tougaard, J. Vac. Sci. Technol. A 8 (1990) 106.
[39] L.E. Davis, N.C. McDonald, P.W. Palmberg, G.E. Riach and R.E. Weber, Handbook of Auger Electron Spectroscopy (Physical Electronics Industries, Eden Prairie, MI, 1976).
[40] L. Hilaire, G.D. Guerrero, P. Légaré, G. Maire and G. Krill, Surf. Sci. 146 (1984) 569.
[41] E. Ticanelli, J.G. Berry, M.T. Paffett and S. Gottesfeld, J. Electroanal. Chem. 258 (1989) 61.
[42] T.T. Tsong, D.M. Ren and M. Ahmad, Phys. Rev. B 38 (1988) 7428.
[43] Y.S. Ng and T.T. Tsong, Surf Sci. 78 (1978) 419.
[44] H. Miura, T. Suzuki, Y. Ushikubo, K. Sugiyama, T. Matsuda and R.D. Gonzales, J. Catal. 85 (1984) 331.
[45] S. Alerasool, D. Boecker, B. Rejal and R.D. Gonzales, Langmuir 4 (1988) 1083.
[46] S. Alerasool and R.D. Gonzales, J. Catal. 124 (1990) 204.
[47] J.A.V. Butler, Proc. R. Soc. London 135 (1932) 348.
[48] A. Schuchowitzky, Acta Physicochim. URSS 19 (1944) 176.
[49] E.A. Guggenheim, Trans. Faraday Soc. 41 (1945) 150.
[50] R. Defay and I. Prigogine, Trans. Faraday Soc. 46 (1950) 199.
[51] R.A. Swalin, Thermodynamics of Solids (Wiley, New York, 1962).
[52] R.A. van Santen and W.M.H. Sachtler, J. Catal. 33 (1974) 202.
[53] P. Wynblatt and R.C. Ku, Surf Sci. 65 (1977) 511.
[54] A.R. Miedema, Z. Metallkde. 69 (1978) 455.
[55] J.K. Strohl and T.S. King, J. Catal. 118 (1989) 53.
[56] W.R. Tyson and W.A. Miller, Surf. Sci. 62 (1977) 267.
[57] L.Z. Mezey and J. Giber, Surf. Sci. 117 (1982) 220.
[58] M. Kelley, J. Catal. 57 (1979) 113.
[59] W.R. Tyson, Can. Met. Quart. 14 (1975) 307.
[60] A.R. Miedema, Philips Tech. Rev. 36 (1976) 217.